Lab on a Chip

Accepted Manuscript

ROYAL SOCIETY OF CHEMISTRY

www.rsc.org/loc

Table of contents entry

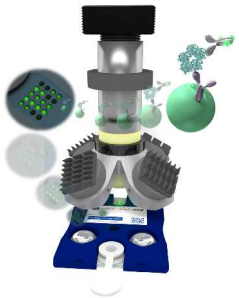

The programmable bio-nano-chip (p-BNC) is an ultra-flexible system for multiplexed and multiclass assays on a universal modular lab-on-a-chip platform for clinical and bioscience applications at the point-of-care.

Lab on a Chip

ARTICLE

Programmable bio-nano-chip system: a flexible point-of-care platform for bioscience and clinical measurements

Received 00th January 20xx,
Accepted 00th January 20xx

DOI: 10.1039/x0xx00000x

www.rsc.org/

Michael. P. McRae,[a] Glennon. W. Simmons,[a,b] Jorge Wong,[a,b] Basil Shadfan,[b] Sanjiv Gopalkrishnan,[c] Nicolaos Christodoulides,[abd] and John T. McDevitt [*abd]

The development of integrated instrumentation for universal bioassay systems serves as a key goal for the lab-on-a-chip community. The programmable bio-nano-chip (p-BNC) system is a versatile multiplexed and multiclass chem- and bio-sensing system for bioscience and clinical measurements. The system is comprised of two main components, a disposable cartridge and a portable analyzer. The customizable single-use plastic cartridges, which now can be manufactured in high volumes using injection molding, are designed for analytical performance, ease of use, reproducibility, and low cost. These labcard devices implement high surface area nano-structured biomarker capture elements that enable high performance signaling and are index matched to real-world biological specimens. This detection modality, along with the convenience of on-chip fluid storage in blisters and self-contained waste, represents a standard process to digitize biological signatures at the point-of-care. A companion portable analyzer prototype has been developed to integrate fluid motivation, optical detection, and automated data analysis, and it serves as the human interface for complete assay automation. In this report, we provide a systems-level perspective of the p-BNC universal biosensing platform with an emphasis on flow control, device integration, and automation. To demonstrate the flexibility of the p-BNC, we distinguish diseased and non-case patients across three significant disease applications: prostate cancer, ovarian cancer, and acute myocardial infarction. Progress towards developing a rapid 7 minute myoglobin assay is presented using the fully automated p-BNC system.

Introduction

Significant progress has been made towards the development of lab-on-a-chip (LOC) devices over the years serving a variety of applications.[1-4] However, few of these devices have obtained widespread commercial and clinical adoption.[5, 6] Traditionally, microfluidics research has relied on cumbersome equipment like syringe pumps and microscopes which are not amenable to point-of-care (POC) settings.[1, 2] Integration of microfluidic and instrumentation components into a unified system remains a central challenge for POC diagnostics.[7, 8] In particular, developing a portable, inexpensive, and sensitive optical detection system is critically important. Recent innovations in manufacturing high quality optoelectronics like complementary metal–oxide–semiconductor (CMOS) and light emitting diodes (LED) have created new opportunities for low-cost and sensitive instrumentation in LOC devices. Further, co-development of the LOC device and associated instrumentation is essential to ensure mutual compatibility of the integrated system.[6, 9] Similarly challenging is creating an automated workflow compatible for non-experts with limited to no human intervention required between sample introduction and data presentation.[10]

A primary design consideration for LOC systems is the method for fluid motivation. Fluid flows can be manipulated in microfluidic devices through a variety of driving forces (*e.g.*, pressure, electric, magnetic, capillary, centrifugal, acoustic) for many purposes (to mix, react, detect, analyze, separate, *etc.*).[11] In particular, the external compression of on-chip fluid-filled pouches or blister packs is attractive for POC applications because all of the necessary reagents can be stored conveniently on the device. In this configuration, fluid flow may be initiated by finger actuation[12] or controlled by an analyzer providing blister actuation.[13, 14] Aside from blood glucose measurements, perhaps one of the most successful POC diagnostics to date, the i-STAT® device, uses pneumatic actuation to control the movement of blood sample through a microfluidic cartridge via external electromechanical interaction from a handheld analyzer.[15] Similarly, Daktari Diagnostics is using a blister actuation approach for their $CD4^+$ and $CD8^+$ T lymphocyte counting device.[16] Our group also has

[a] Department of Bioengineering, Rice University, Houston, TX, U.S.A.
[b] Department of Chemistry, Rice University, Houston, TX, U.S.A.
[c] Department of Mechanical Engineering, Rice University, Houston, TX, U.S.A.
[d] Department of Biomaterials and Biomimetics, New York University College of Dentistry, New York, NY, U.S.A.
* Corresponding author, E-mail: mcdevitt@nyu.edu
Electronic Supplementary Information (ESI) available: [details of any supplementary information available should be included here]. See DOI: 10.1039/x0xx00000x

prior experience using blisters for on-chip storage and motivation of fluids.[17, 18] Rigorous control of fluid flow is critical to the accuracy and precision of high fidelity and quantitative bioassays. Further, the ability to customize multi-step assays with various flow rates optimized for reaction kinetics is highly desirable to service a broad range of clinical tests. Little information is currently available in the literature about the accuracy and reproducibility of customizable and controlled flows resulting from blister actuation in the context of microfluidic-based bioassay systems.

Outside of integrated blister pack LOC structures, several groups have demonstrated significant progress towards integration and automation of assay systems. For example, Sia and colleagues have developed a low-cost mobile device with laboratory-quality results for testing HIV in remote settings.[19] Cho and co-workers created a fully integrated lab-on-a-disc and portable analyzer that performs simultaneous biochemical analyses and immunoassays from whole blood.[20] The Walt group has designed a platform for automated and multiplexed testing of salivary samples for the diagnosis of respiratory diseases.[21] The Wheeler group developed an immunoanalyzer based on a digital microfluidics platform.[22] Bau and colleagues designed a fully automated reader and a self-contained disposable cassette for nucleic acid detection.[23] Singh and co-workers developed a microchip electrophoretic immunoassay and associated instrumentation for the quantitation of protein biomarkers in saliva.[24] Lee's group developed a self-powered, integrated microfluidic blood analysis system that eliminates the need for external connections to deliver and analyze whole blood.[25] Ligler *et al.* developed an easy-to-use portable array biosensor system that can analyze multiple samples for multiple analytes.[26] Yager's DxBox performs differential diagnosis of infections using a disposable flow-through membrane immunoassay microfluidic card.[27] Lochhead's MBio system delivers multiplexed immunoassay results using a novel multimode planar waveguide and a USB-powered reader.[28] Heath's innovative barcode chip platform accomplishes simultaneous multi-class and multiplexed quantitation of proteins and metabolites from single cells through spatial addressing of capture regions.[29] Qin's volumetric bar-chart chip performs ELISA using nitrogen gas competition between the sample and an internal control to direct the flow of an visually positive or negative ink bar indicator, overcoming the ambiguity and environmental effects that affect some POC tools such as lateral flow assays.[30] Several groups are integrating mobile phones with LOC devices, leveraging their imaging capabilities, connectivity, and ubiquity for performing various biochemical assays in resource-limited settings. Significantly, Ozcan's team has developed a mobile phone fluorescence microscope with machine learning software for automated detection of *Giardia* cysts.[31] Yager's work integrates low-cost paper-based devices and cell phone imaging for the goal of increasing access and affordability to healthcare.[32] The Whitesides group has developed a handheld device that performs electrochemical testing and transmits data to "the cloud" using a mobile phone.[33] Demirci and co-workers are using cell phone imaging with microchip enzyme-linked immunosorbent assay (ELISA) to detect the ovarian cancer marker HE4 at the POC.[34]

While there are numerous successful applications of LOC devices targeting single application verticals, there remains less progress in the creation of broadly responsive universal bioassay systems for POC use.[9, 35] The expense and time associated with design, fabrication, testing, and validation serve as barriers for dedicated single-class bioassay systems.[36] There is a strong need for universal modular testing platforms designed for non-expert users that can quickly and efficiently provide the clinical biosensing community with strategic disease-specific panels.

In this report, we provide a systems-level perspective of the programmable bio-nano-chip (p-BNC)[17, 18, 37-43] technology with an emphasis on fluid motivation, device integration, and automation. The cartridge design optimization and rationale will be published elsewhere. The versatility of the device is highlighted by the detection of eight different analytes isolated from human serum samples across three disease applications, prostate cancer, ovarian cancer, and acute myocardial infarction (AMI). Further, the device's basic functionality is demonstrated for an in development rapid myoglobin assay.

Materials and Methods

Materials

The p-BNC cartridge design was inspired by laminate-based and fully integrated prototypes described previously.[41] The injection molded plastic disposable cartridges for this study were manufactured by MiniFAB (Scoresby, Victoria, Australia). Sterile PBS encapsulated in foil blister packs and mounted on the cartridges served as the washing buffer and on-board fluid source. Glass fiber conjugate pad was purchased from Millipore (Bedford, MA, U.S.A.) and was cut into 2 × 15 mm rectangles, spotted with detecting antibody reagents, and embedded in the cartridges. Capture and detection reagents were prepared with SuperBlock (PBS) Blocking Buffer from Thermo Fisher Scientific (Waltham, MA, U.S.A.). The following were purchased from Edmund Optics (Barrington, NJ, U.S.A.): Nikon CFI Plan Fluor 4× objective lens (part no. 88-378), InfiniTube™ FM-100 (0.5×) tube lens (part no. 58-309), InfiniTube™ FM Nikon CFI60 objective adapter (part no. 58-315), InfiniTube™ mounting C-clamp (part no. 57-788), emission filter (part no. 67-017), four excitation filters (part no. 67-028), *z*-axis precision compact motorized stage (part no. 88-554), PixeLINK® PL-B957-BL camera (part no. 64-183), 1″ steel post (part no. 59-751), and post holder (part no. 58-976). Four high-power blue (490 nm) LEDs (part no. M490D2), four aspheric condenser lenses (part no. ACL2520-DG15-A), and four SM1 lens tubes (part no. SM1L05) were purchased from Thorlabs (Newton, NJ, U.S.A.). Four LED heat sinks (part no. LPD25-4B), mounting tape (part no. LT-03), and two 350 mA BuckPuck™ DC LED drivers (part no. 3021-D-I-350) were purchased from Luxeon Star LEDs (Brantford, Ontario, Canada). Two size 14 captive linear actuators (part no. 35H4N-2.33-907) were purchased from Haydon Kerk Motion

Solutions, Inc. (Waterbury, CT, U.S.A.). Three EasyDriver stepper motor drivers (part no. ROB-10267), Arduino Pro Mini microcontroller board (part no. DEV-11113), FTDI cable (part no. DEV-09718), and two 0.5″ force sensitive resistors (part no. SEN-09375) were purchased from SparkFun Electronics (Niwot, CO, U.S.A.). Two LM358 op-amps (part no. LM358NFS-ND) were purchased from Digi-Key (Thief River Falls, MN, U.S.A.). Four ¼″-20 carriage bolts (part no. 92356A558) and 0.5″ thick acrylic sheets (part no. 8560K266) were purchased from MacMaster-Carr (Elmhurst, IL, U.S.A.). The acrylic sheet was cut and patterned with a CO_2 laser cutter (Universal Laser Systems, Scottsdale, AZ, U.S.A.). A 7″ touchscreen monitor (Touch 2) was purchased from Mimo Monitors (Princeton, NJ, U.S.A.). An embedded PC (part no. GB-BXi3-4010) running Windows® 7 (64-bit) was purchased from Gigabyte Technology Co., Ltd. (New Taipei City, Xindian District, Taiwan). A monochrome CMOS camera (Grasshopper3) was purchased from Point Grey (Richmond, British Columbia, Canada).

A custom printed circuit board (PCB) for hardware integration was designed using PCB Artist™ software and manufactured by Advanced Circuits (Aurora, CO, U.S.A.). Custom 3-D printed parts (cartridge loading mechanism and supports for actuators, camera board, and PCB) were designed in SolidWorks® 2013 3D CAD software (Waltham, MA, U.S.A.) and produced by 3D Systems ProJet™ 3000 (Rock Hill, SC, U.S.A.). The protective enclosure and supporting frame was designed and manufactured by XACTIV (Fairport, NY, U.S.A.). All software for the analyzer was developed in MATLAB® 2014a (Natick, MA, U.S.A.) and compiled as a standalone application using MATLAB® Compiler Runtime.

Verification of flow rates

To verify the blister actuation algorithm, a method for measuring flow rates was developed. Prototype blisters were fabricated from a dome-shaped aluminum mold made via vacuum thermoforming polycarbonate (McMaster-Carr, Elmhurst, IL, U.S.A.). The blister actuator tips were cast in optically clear epoxy, Norland Optical Adhesive 81 (Norland Products Inc., Cranbury, NJ, U.S.A.), from the same dome-shaped mold. Negative thermoforming molds were milled on a Haas Office Mill 2A CNC machine (Harvey Tool Company, LLC., Rowley, MA, U.S.A.), and a single through-hole was drilled in the center of the cavity for integration with a vacuum. Blisters were filled with 1 mL of blue food dye and closed with double-sided adhesive (DSA) polyester film (3M Company, St. Paul, MN, U.S.A.) and another polycarbonate layer. A specialized microfluidic test structure with meandering channels was designed via xurography (**Supplemental Fig. S1**). Top and bottom capping layers were made from 3M™ AF4300 polyethylene terephthalate (PET), and the meandering channels were patterned in a single adhesive layer of DSA. Geometry-adjusted actuation software was implemented on a standalone blister actuator platform (**Supplemental Fig. S2**). Five runs at each target flow rate (10, 50, and 100 µL/min) were performed. Blisters were completely actuated for the 50 and 100 µL/min tests and partially actuated (200 µL) for the 10 µL/min tests. Video of the fluid flow (blue dye against a white background) was captured with Canon EOS Revel T1i camera (Canon, Inc., Ōta, Tokyo, Japan). Video analysis software developed in MATLAB calculated the flow rate by tracking the velocity of the leading edge of the blue dye within a channel of known volume. The resulting flow rates were then signal averaged, and the mean and standard deviations of the signal averaged flow rates were calculated as well as the coefficients of variation (CV) of the five runs.

Device multi-functionality

Using the p-BNC disposable cartridges and prototype analyzer, human clinical samples were tested for prostate cancer, ovarian cancer, and AMI. Informed consent was obtained from all participating subjects prior to testing. In each disease area, “case” and “non-case” patients were analyzed using multimarker panels. For prostate cancer, human serum samples were obtained from a female control and a suspected prostate cancer male patient. The prostate cancer panel, containing total and free prostate specific antigen (PSA) bead sensors, attempts to distinguish between healthy and suspected prostate cancer cases. Mouse monoclonal anti-human total PSA (catalog no. 10-1122) (Fitzgerald Industries International, Acton, Massachusetts, U.S.A.) and free PSA (catalog no. M167) (CalBioreagents, San Mateo, CA, U.S.A) antibodies were conjugated to the bead sensors by reductive amination for target capture. Matched pairs (catalog no. 10-1123) from Fitzgerald Industries International were conjugated to AlexaFluor-488® for detection using the AlexaFluor-488® protein labeling kit from Life Technologies (Carlsbad, CA, U.S.A.) following manufacturer protocols. For ovarian cancer, human serum samples were obtained from a recent study, and a 2-plex panel was developed using protocols previously described.[41] The panel, containing cancer antigen 125 (CA125) and human epididymis protein 4 (HE4) bead sensors, attempts to distinguish between a healthy female control and a late-stage ovarian cancer patient. Human serum samples for cardiac testing were obtained from a recent clinical study following chest pain patients who presented to the emergency room with symptoms of acute coronary syndrome. The cardiac panel, containing bead sensors for cardiac troponin I (cTnI), creatine kinase MB (CK-MB), myoglobin (MYO), and N-terminal pro-brain natriuretic peptide (NT-proBNP), attempts to distinguish a non-case chest pain patient and a patient diagnosed with AMI. Mouse monoclonal anti-human antibodies were conjugated to the bead sensors by reductive amination for target capture, and matched pairs were conjugated to AlexaFluor-488® following manufacturer protocols. Further details of the cardiac assay will be reported elsewhere. For each disease application, serum was separated from whole blood at the respective clinical sites and stored in aliquots at -80°C. The undiluted samples were thawed immediately before introduction to the cartridge, and an aliquot of 100 µL of serum was used for each assay.

All fluid manipulations were handled by the portable analyzer. Case and non-case assays were performed once for each disease application. Images were captured using an

exposure time of 500 ms for prostate cancer and 100 ms for cardiac and ovarian cancer panels. Median pixel value of the background, defined as the entire image excluding the bead sensors, was subtracted for all images. Display intensities range 0 to 1000 for ovarian cancer and 0 to 2000 for cardiac and prostate panels. Mean fluorescence intensity (MFI) was calculated for each biomarker type via an annular region of interest method where the signal was averaged within the annulus between the bead outer diameter and 90% of the bead radius.

Rapid myoglobin assay

MYO-specific antibodies and standards were acquired from Meridian Life Sciences Inc. (Memphis, TN, U.S.A.). AlexaFluor-488® was conjugated to MYO (clone 7C3) using AlexaFluor-488® protein labeling kit (Invitrogen, Eugene, Oregon, U.S.A.). Goat anti Mouse IgG (H + L) (R-PE) antibodies from Fitzgerald Industries International were conjugated to the beads as positive controls. Reagent pads were functionalized with a cocktail of detecting antibody reagents and installed in the cartridge's reagent pad chamber. Twelve MYO beads, four positive calibrator beads, and four negative calibrator beads were loaded by hand into the 4 × 5 chip. All fluid manipulations were handled by the automated portable analyzer prototype. Images were captured using exposure time of 1000 ms. Median pixel value of the background was subtracted for all images. MFI was calculated for each biomarker type via an annular region of interest method where the signal was averaged within the annulus between the bead outer diameter and 90% of the bead radius. A dose response curve (5-parameter logistic) was constructed for MYO using a concentration range 0 ng/mL to 2500 ng/mL. MFI was recorded for a single run for each dilution, and intra-assay standard deviation was calculated from 12 redundant MYO bead sensors.

Results and discussion

p-BNC system

Fig. 1 shows the p-BNC assay system comprised of a disposable assay cartridge and portable analyzer. The disposable cartridge (**Fig. 1A**) is a LOC microfluidic platform for multiclass and multiplexed quantitation of bioanalytes. The cartridge is self-contained, integrated, and has reagents conveniently embedded for usability at the POC. The labcard device contains analyte-specific antibodies bound to 280 µm diameter agarose beads supported in a plastic flow-through microchip described previously.[44] This design provides convective transport to the interior of the porous beads, efficient diffusion distances, and short depletion layers which improves sensitivity compared to flat microfluidic channels.[45] Forming immunocomplexes throughout a 3-D matrix allows the signal to be layered via a higher density of reagent capture within a 3-D lattice as opposed to 2-D capture in the case of lateral flow devices. This mini-sensor ensemble is capable of multiplexing fluorescence immunoassays for proteins, oligonucleotides, and small molecules, outperforming laboratory-based ELISA in terms of analysis time, limits of detection, and ease of use.[37] The p-BNC is compatible with both competitive and non-competitive assay formats, and the ability to pick and place bead sensors and reagent pads allows ultimate flexibility in a unified form factor.

The p-BNC analyzer (**Fig. 1B**) optically images the p-BNC's bead sensors and automates sample handling that would otherwise have been performed by a trained lab technician. The automation of sample and reagent handling not only eliminates the need for trained technicians and manual manipulations, but also reduces the variability between tests and across test sites allowing for quality standard measurements with a high degree of reproducibility. Further, the analyzer performs automated data analysis on the

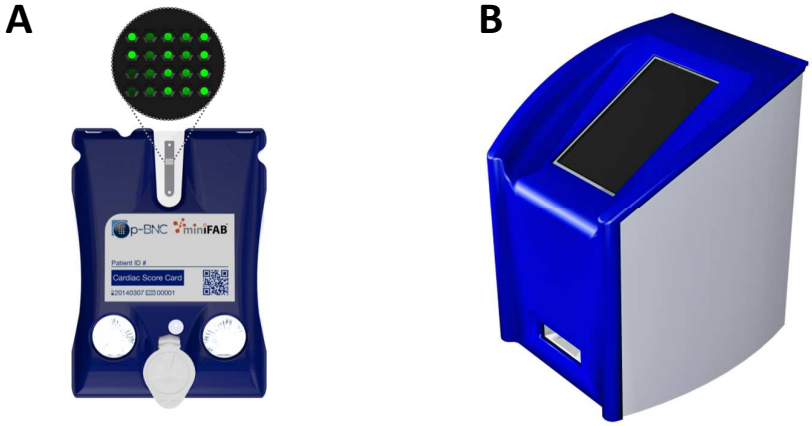

Fig. 1. (A) Illustration of the p-BNC disposable cartridge with bead sensors magnified. (B) Illustration of the portable analyzer.

acquired images, converts the image into usable data (*i.e.*, biomarker concentrations), and relays the data to disease-specific machine learning algorithms for diagnosis and prognosis. Since multiple disease applications are represented in this work, an in-depth description of these diagnostic and prognostic algorithms and their clinical interpretation is out of scope. However, future studies will provide in-depth clinical coverage for this new instrumentation here presented.

Disposable cartridges

The labcard device featured in this work was created in two major stages. First, laminate-based prototypes were developed using a rapid prototype approach.[41] More recently, an injection molded version of the laminate prototype was developed in collaboration with commercial partners where the manufacturing processes established to date are compatible with scaling up to high volume and automated production. **Fig. 2** depicts the cartridge's major features and internal microfluidic circuitry. The main fluidics module consists of an injection molded cartridge body capped with adhesive layers designed for scalable manufacturing. The bio-specimen (*e.g.*, serum or saliva) is introduced into the sample loading port. Fitted to the main fluidic body, this plastic piece is the inlet and reservoir for sample introduction. An easy-to-use adhesive cap is tethered to the loading port and sealed prior to initiating the assay sequence. The user-configurable reagent pad chamber is accessed through an opening on the top face of the card, allowing the assay to be easily reconfigured via a conjugate pad with dried reagents (*e.g.*, detecting antibody). The reagent pad is a glass fiber conjugate pad cut into 2 × 15 mm rectangles. The glass fiber material serves as a high surface area support for the detecting antibodies. The pad's high aspect ratio facilitates repeatable and efficient elution of the reagents. Two foil blister packs containing buffers serve as the on-chip fluid source. Blister puncturing mechanisms on the molded layer rupture the blisters upon actuation and facilitate fluid flow into the cartridge. Self-contained waste chambers on either side of the bead sensor array store the used reagents and bio-specimen for safe and convenient disposal of the device. The sensor region shown here is comprised of a 4 × 5 array of flow-through microwells which are "programmed" by the placement of analyte-specific agarose bead sensors. The chip wells are tapered hexagonal containers; the six walls have a tapered angle of 54.7° with respect to the normal and are designed to contain a single 280 µm diameter bead. This critical design feature allows for pressure-driven flow to deliver analytes into the porous beads via convective transport, effectively layering signal within the 3-D agarose lattice.[42] While larger bead array matrices have been explored in the prototyping phase of development, the 4 × 5 matrix was selected based on a variety of factors. For instance, the well spacing is comfortably within plastic injection molding manufacturing capabilities, and this particular configuration fits within the desired field of view of the analyzer. For cell counting and differentiation applications, this sensor modality is simply swapped with a membrane capturing element (not shown). The cartridge shell protects the blisters during shipping and handling, contains alignment features for mechanical stabilization within the portable analyzer, and provides a surface for the cartridge label which contains patient ID, cartridge serial number, and a unique QR code for identification.

The dimensions of the cartridge are largely dependent on the volume of sample and reagents necessary for the assay. The sample loop was designed to facilitate 100 µL of sample, and the self-contained waste chambers were designed to store the sample volume and about 2 mL of buffer from the blister packs. Further, the dimensions and positioning of the cartridge components allows for external manipulation of the blister packs via the actuators without interfering with LED excitation and optical instrumentation. Similarly, the bead array is centered between symmetrical waste chambers so that the optical assembly may be centered within the instrument. The sample loading port is located opposite the bead sensors so that it hangs outside of the instrument, minimizing the risk of leakage and potential contamination inside the instrument. A more detailed description of the cartridge design will be covered in a future report.

Portable analyzer

The p-BNC analyzer is approximately 9″ × 9″ × 12″ (length × width × height), weighs less than 15 lbs, and has four main functions: fluid motivation, optical detection, automated data analysis, and human interface. **Fig. 3** highlights the major components that facilitate these functions.

Fluid motivation

Flow rate plays an important role on the effect on analyte capture in most microfluidic systems. Our previous work explored the effect of various sample flow rates on analyte capture within the p-BNC system.[45] The porous bead substrates have a unique multiple kinetic regime in which the exterior of the bead is reaction-limited while the interior of the bead is transport-limited. Thus, the amount of captured material on the bead largely depends on the delicate interplay between these two effects. Defining the flow rate conditions in the p-BNC is an important assay optimization step, and various factors are considered including volume limitations, time constraints, and performance. Therefore, it is important to develop instrumentation that can deliver accurate and repeatable flow rates.

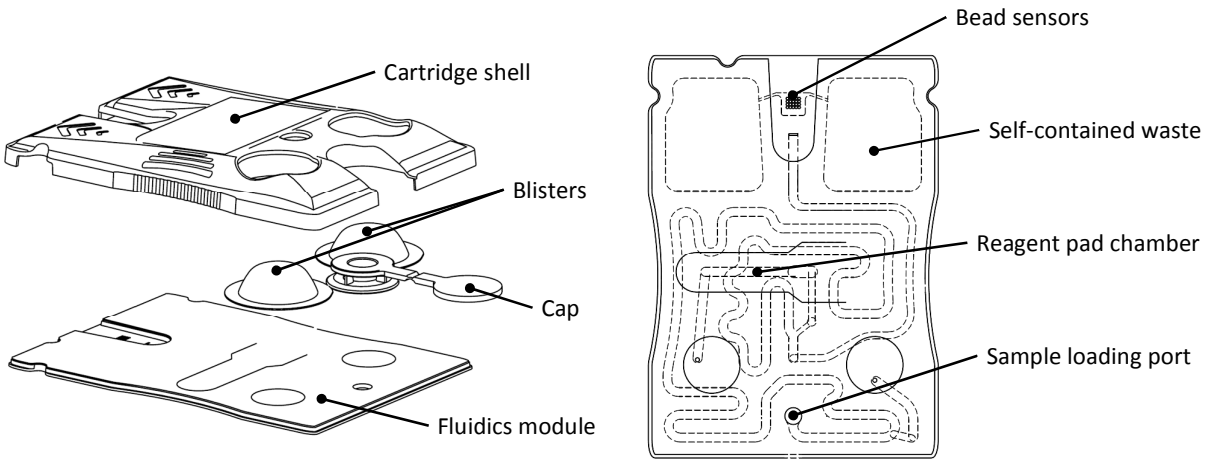

Fig. 2. Drawings of the p-BNC disposable cartridge in an exploded view (left) and assembled top view (right).

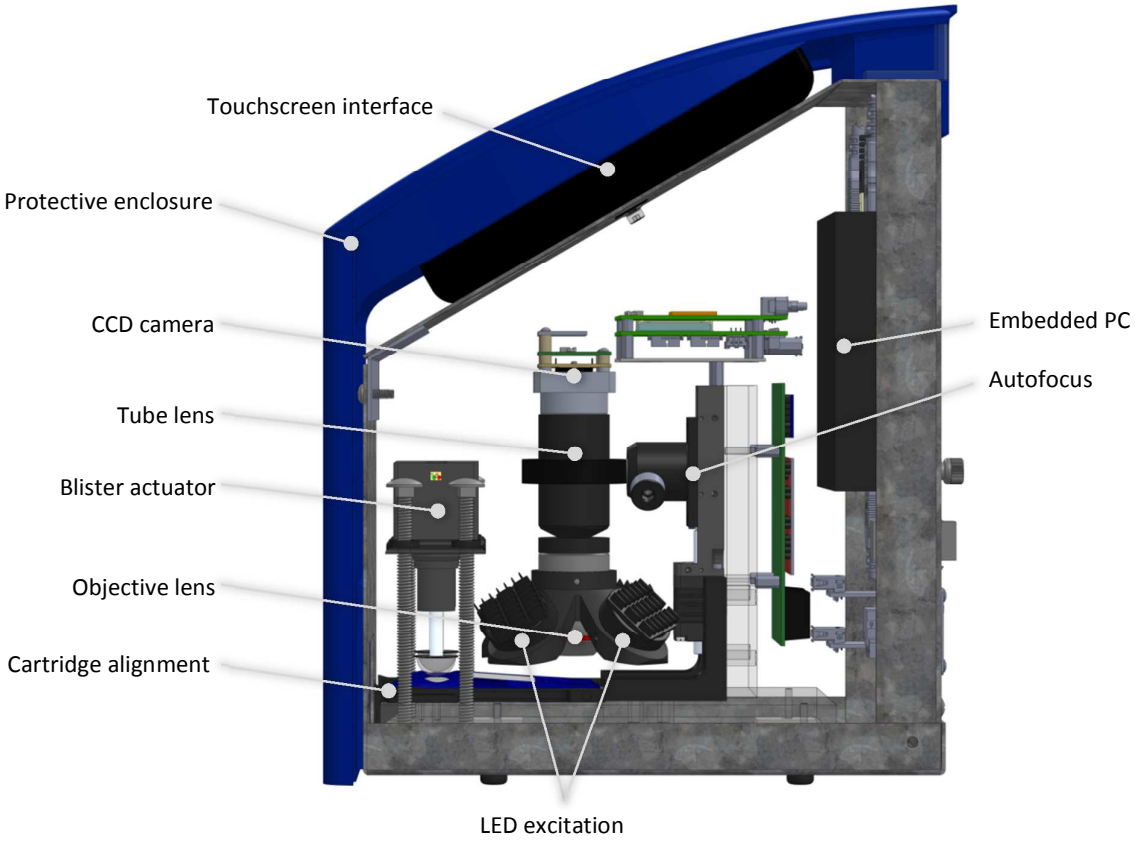

Fig. 3. Schematic illustration highlighting the p-BNC analyzer's major features.

The p-BNC system was designed for ultimate convenience at the POC; thus, its liquid reagents are located directly on the cartridge in the form of blister packs which hermetically seal them with foil to prevent contamination and evaporation. Upon actuation, the blister packs rupture and release their contents into the cartridge in a controlled fashion. Two key innovations have ensured repeatability of these events: force sensitive feedback for detecting the blister burst and geometry-adjusted actuation rate for delivering accurate and constant flow rates. The blister actuation module features two linear actuators oriented vertically over each of the cartridge's blisters. Force sensitive resistors (FSRs) detect when the actuator tip makes contact with the blisters and when the blister bursts, releasing its contents into the cartridge. Dome-shaped blister actuator tips attached to the surface of the FSRs facilitate the actuator's mechanical interface with the blisters.

The p-BNC assay uses pressure-driven flow via the actuation of blister packs to perform multiple steps at various programmable flow rates. One challenge with this approach is the difficulty in delivering accurate and constant flow rates due to the geometry of the blister. As the actuator compresses the dome-shaped blister, the contact surface area increases; thus, the flow rate increases as actuation into the blister progresses. However, with careful manipulation of the actuation rate, accurate and constant flow rates can be achieved. In this context we developed a mathematical model of blister and actuator geometry interaction to deliver constant and accurate flow rates. The dome shape of the actuator tip was chosen such that it approximates the geometry of the blister, thus simplifying the algorithm for geometry-adjusted actuation rate (*i.e.*, by using a dome-shaped actuation surface, contact surface area increases approximately linearly with actuation depth). Another advantageous property of the dome-shaped tip is that a curved actuation surface provides uniform and predictable deformation of the blister, whereas a flat actuation surface caused unpredictable buckling and folding of the blister's foil.

Here, blister actuation was modeled as the interaction of two spherical caps (**Fig. 4A**) corresponding to the blister and the actuator tip. The total volume of the blister is given by the volume of the spherical cap in **Eq. 1**.

$$V = \frac{\pi h^2}{3}(3r - h) \qquad \textbf{Eq. 1}$$

where r is the radius of the sphere and h is the height of the spherical cap. To determine the ejection volume as a function of actuation depth, the interaction of two spherical caps was modeled. The actuation depth, z, refers to the location of the actuator tip between the apex of the blister ($z = 0$) and the bottom of the blister ($z = h$). Here, we simplify by assuming the blister and actuator have identical geometry; thus, the volume ejected from the blister at actuation depth, z, is equal to the interaction volume of two spherical caps at depth z / 2. Then, the volume ejected per step of the linear actuator is

$$\frac{dV}{dz} = \frac{1}{4}\pi z(4r - z). \qquad \textbf{Eq. 2}$$

The volumetric flow rate is given by $Q = dV/dz * dz/dt$, where the desired constant flow rate Q is generated by applying the actuation rate, dz/dt. To generate constant flow of reagents, the stepper motor driver sends alternating high and low voltage signals to the motor such that the time delay to the linear actuators, dt, scales with the volume ejected as actuation depth into the blister increases. Flow rates were obtained from five runs, and these time delay instructions were finally adjusted using a scaling factor to achieve constant flow rate at the desired target.

To verify the actuation method, flow rates were measured by tracking the fluid velocity of dye ejected from prototype blisters using a custom designed microfluidic card with meandering channels (**Supplemental Fig. S1)**. **Fig. 4B** shows images of the blister actuation process, and **Fig. 4C** shows the results obtained using custom video analysis software. High, medium, and low flow rates (100, 50, and 10 µL/min) were targeted by the blister actuator software. The average flow rates measured were 98, 50, and 10 µL/min with CV 4, 4, and 8% for the 100, 50, and 10 µL/min tests, respectively. Relatively low CV and constant flow rate profiles demonstrate adequate control over fluid delivery using this blister actuation approach.

Optical detection

The p-BNC analyzer uses a compact fluorescence microscope system for imaging fluorescently labeled beads. The illumination module consists of four equally spaced, obliquely oriented (45° from normal) blue LEDs (490 nm) that are filtered (482.5 nm center wavelength bandpass filter) and relayed to the p-BNC chip via aspheric condenser lenses with a diffuser surface. One of the main challenges in using an off-axis illumination system is achieving uniform illumination intensity across the entire bead array. Illuminating with four symmetrically spaced LEDs offered superior uniformity over 2-

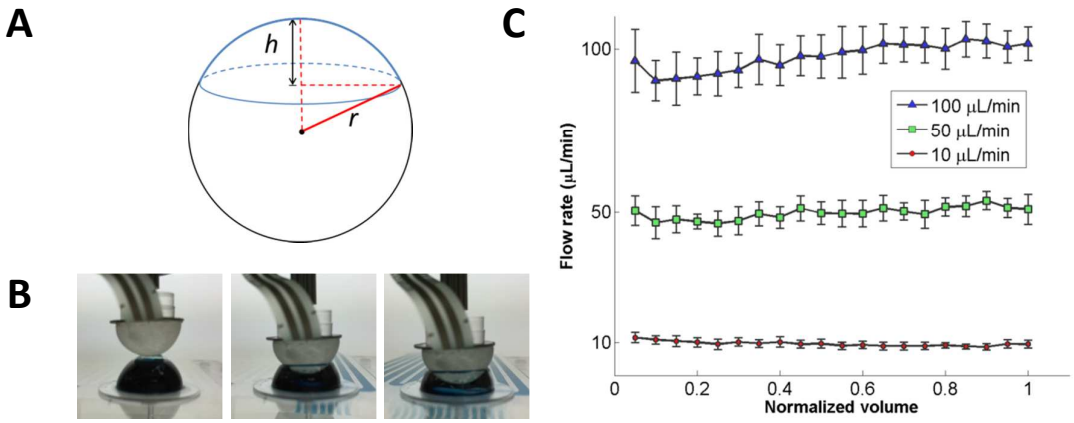

Fig. 4. (A) Spherical cap geometry. (B) Images of the blister actuation process displaying the actuator compressing the blister at various heights. (C) Flow rate verification results showing mean flow rates and standard deviation (error bars) for five runs at each target flow rate as the fluid (normalized volume) is ejected from the blister.

and 3-LED configurations. Additionally, improvements in signal-to-noise and signal-to-background ratios have been observed with increased illumination power, suggesting the potential for improvements in sensitivity at low concentrations. Since diffuser surfaces in the aspheric condenser relay lenses limited the illumination power in favor of increased uniformity, multiple LEDs were necessary to provide adequate illumination intensity. The compact lens assembly consists of an objective lens, emission bandpass filter (534.5 nm center wavelength), and tube lens. An off-the-shelf objective lens was selected with 4× magnification and 0.13 NA for its availability, performance, and form factor. Similarly, the tube lens provides a convenient inline optical assembly, condenses optical path length, and demagnifies the image (0.5×). A monochrome CCD camera (Sony ICX285 image sensor) was selected for its low-profile board-level configuration and USB compatibility. While the analyzer featured here uses a CCD imager, the modular optical assembly can accept cost-effective and high-performance CMOS image sensors. The optics module is mounted to a linear motorized stage that translates the entire assembly for focusing. An autofocusing algorithm works by translating to the vertical position with maximum variance in a region of interest containing the positive calibrator beads as focal aids.

Automated data analysis

The p-BNC's image analysis software implements novel computer vision methods for detecting the location of beads using a Gabor annulus approach and analyzing pixels according to various regional and intensity-based parameters. The Gabor annulus method, based on the advantageous properties of Gabor wavelet filters, is a popular method for recognizing patterns.[46] This filter is convolved across the image, resulting in a large response in areas where an image's features or patterns match their specific scale, orientation, and location. In other words, the filters are fine-tuned to recognize beads, and the alignment of the beads and the Gabor annulus filter results in a large response at the beads' centroids. **Fig. 5** shows the main steps of the image analysis process that is applied to each bead individually. First, the derivative of the raw image isolates the bead's edge from the background and the bead interior. Then, multiple Gabor annuli are formed with slight variations in radius, frequency, and standard deviation parameters. Using a range of Gabor annulus filters with different properties provides broader coverage for recognizing underlying patterns in the image;[47] here, the wavelet properties are tuned to account for the size distribution of beads. The filters are convolved across the image, and the convolution responses are normalized and aggregated. The centroid of the bead is determined by locating the maximum aggregate response. The bead's outer radius is then mapped by revolving an intensity profile about the bead centroid and fitting a circle to the resulting coordinates that correspond to the greatest rate of change in pixel intensity. The distribution of signal across a bead is typically nonuniform, exhibiting strong signal along the outer radius and weak signal towards the center. Averaging the pixels over the entire bead region leads to lower signal and higher intra-bead variance. Therefore, an annular region of interest (ROI) method was developed to exclude low signal pixels in the bead center and instead analyze the pixels around the edges of the bead. Once the ROI is mapped, the mean signal is extracted for each bead, and a two-sided Grubbs' test for outliers is applied to the redundant bead sensors using a significance level of $\alpha = 0.10$.

Human interface

The cartridge slot contains a 3-D printed alignment feature that accepts the disposable and snaps the cartridge into precise alignment with the blister actuators and optics module. The portable reader also features a touchpad user interface, a fan and vents for cooling, and a removable rear panel with electronic interfaces for the following: barrel power inputs for powering the embedded PC and LED module, two USB A-A connectors, an RJ45 adapter for ethernet connection, and an HDMI adaptor for displaying on an external monitor. Data may be transmitted to a server via wireless internet or manually via USB. The exterior of the p-BNC instrument supports, encloses, and protects the instrumentation modules from the environment and prevents background light from entering the analyzer.

Device operation

With the bead sensors pre-loaded into the cartridge, the user deposits ≥ 100 µL sample (serum, saliva, or urine) into the sample loading port and seals the cartridge cap. The cartridge passively wicks the sample through the main fluidic channel and precisely meters 100 µL to be used in the assay. The user then inserts the card into the analyzer and starts the assay in which the remaining steps are performed automatically by the portable analyzer. The sample delivery is controlled by

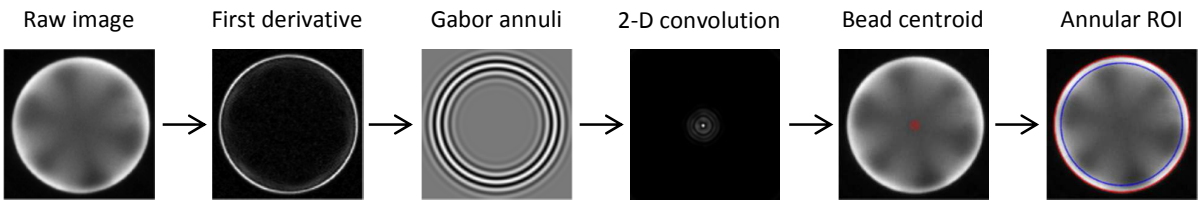

Fig. 5. Summary depicting major steps (left to right) of the automated image analysis routine for a single bead. A collection of Gabor annulus filters are applied to the derivative of a raw image via 2-D convolution to locate the centroid of the bead. Once located, the annular ROI method averages the pixel intensity near the bead's outer radius where signal is greatest (far right, the ROI shown between red and blue circles).

compressing the right blister while the detecting antibody delivery is controlled by compressing the left blister. To release the blister contents, the blister actuator steps down towards the cartridge until the FSR detects the top of the blister. The actuator compresses the blister until the blister's foil is ruptured by the sharp puncture mechanism underneath the blister. The bursting event is detected by sensing a change in voltage across the FSR. Next, the blister actuator compresses the blisters according to a geometry-adjusted actuation rate.

The analyzer can perform an extensive menu of assays with customizable flow protocols. The two general fluid profiles are incubation and washing. Incubation steps utilize slow flow rates (1-50 µL/min) to allow adequate binding between antibodies and antigen in the sample. Wash steps are performed at faster flow rates (100-250 µL/min) to remove unbound reagents from the sensor array. For more details on the flow direction and fluid routing through the cartridge, refer to **Supplemental Video 1**. Once the assay steps are complete, the chip is imaged using the analyzer's compact fluorescence microscope. The analyzer's software performs automated image analysis to convert bead signal intensity to biomarker concentration, and these concentrations are then relayed to machine learning algorithms for disease diagnosis and prognosis. After completion of the measurement, the used cartridge, which has built-in and self-contained waste storage, is ejected from the analyzer and can be placed in an appropriate biohazard waste container.

This p-BNC technology has many potential applications spanning a diversity of consumers. Among these envisioned markets is the R&D sector which requires flexibility to develop customized biomarker panels. The p-BNC provides this flexibility via an "open-source" format in which the device "programming" steps are completed by the R&D consumer. Currently, this programming step involves manually loading the beads into the cartridge using tweezers and a dissecting microscope and depositing a glass fiber conjugate pad into the reagent pad chamber. Automated bead placement technology for fully developed assays is currently in development, and R&D users are expected to take advantage of both automated and manual methods for programming the cartridges. The p-BNC chip has microcontainers for 20 beads. Theoretically, 20 different biomarkers could be assayed simultaneously; however, the multiplexing ability of the p-BNC is limited by the specificity and cross-reactivity of the assay developer's reagents. It is also advantageous to have biomarker redundancy in the panel because averaging signal from multiple beads improves the accuracy and precision of the assay. While blister packs containing PBS are currently mounted on the cartridge during the manufacturing process, future R&D applications may require customizable blister packs sold separately and mounted to blank cartridge bodies with double-sided adhesives.

Multifunctional tool for clinical and bioscience measurements

The system featured here is the most recent development in the p-BNC technology which has been in development over the past years. The purpose of this study is to show proof of concept for an integrated and automated bioassay platform with similar performance to previous work conducted in a less integrated (*i.e.*, "macro-scale") manner. As such, accuracy and reproducibility studies for a broad coverage of clinical applications on this new instrument is out of scope at this time and will be featured with greater focus in future publications. Previous work on the macro-scale system reports biomarker ranges and limits of detection for a variety of applications[42] as well as assay performance for specific applications such as drugs of abuse,[48] cardiac heart disease,[49] and ovarian cancer.[41] The new instrumentation here described yields comparable performance to prior lab-based equipment previously reported.

One major hurdle for clinical translation and widespread adoption of a new LOC device is its ability to be easily re-tasked for new applications. To demonstrate the p-BNC system's multi-functionality, a series of in development assays were performed using human serum samples covering three distinct disease applications: prostate cancer, ovarian cancer, and AMI. **Fig. 6** shows data collected for each disease area. The prostate cancer panel (**Fig. 6A**) shows stronger signal from total PSA beads in the suspected prostate cancer patient than the female control and modest increases in free PSA signal. This proof of principle experiment demonstrates the assay's ability to discriminate prostate cancer from healthy controls. In the ovarian cancer panel (**Fig. 6B**), HE4 exhibits substantially higher signal for the late-stage ovarian cancer patient versus the healthy control while showing slightly lower signal in CA125. This example highlights the importance of multiplexed panels in the diagnosis of ovarian cancer. While CA125 is considered the gold-standard marker for prognosing ovarian cancer, a single-marker CA125 test may have reported a false negative result for this late-stage ovarian cancer patient. In the four-plex cardiac panel (**Fig. 6C**), increases in fluorescence intensity are observed between the non-case chest pain patient and the AMI patient for all cardiac biomarkers (cTnI, CK-MB, MYO, and NT-proBNP). This suggests that the p-BNC cardiac panel could detect AMI from non-case chest pain patients in the emergency room. One limitation of the current p-BNC cartridge is that it is not yet configured for interrogating whole blood, and modifications to the cartridge design are necessary to facilitate whole blood analysis. These modifications involve adding inline filtering elements and are now in progress. Although qualitative and in need of more rigorous characterization efforts to show actual clinical utility, this compilation of data reveals the flexibility inherent in the p-BNC system in which different configurations of bead ensembles can be used to reprogram the chip so as to cover alternative disease indications.

Rapid myoglobin assay

Myoglobin, a biochemical marker of myocardial injury, is useful for diagnosing AMI due to its rapid kinetics relative to other cardiac biomarkers.[50-52] Serum myoglobin levels may be elevated within 1 to 2 hours of myocardial death while other

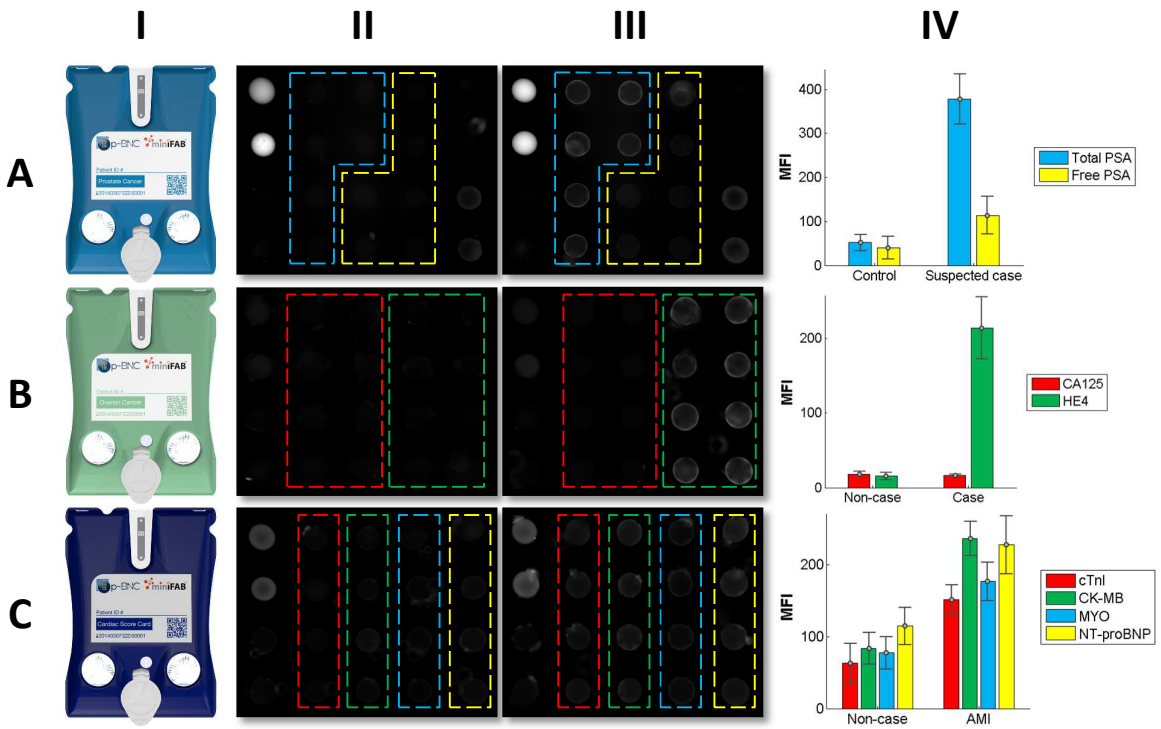

Fig. 6. Multi-functionality of the p-BNC system showing data obtained with injection molded cartridges (I) and portable analyzer prototype for three clinical applications: prostate cancer screening (A), ovarian cancer screening (B), AMI diagnosis (C). Fluorescent photomicrographs in II and III represent non-cases/controls and cases, respectively. All three devices include positive (bright beads) and negative controls (dark beads) at the left most and right most extremes of the bead array (not outlined). Two biomarkers were measured for prostate cancer: total PSA (blue) and free PSA (yellow); two for ovarian cancer: CA125 (red) and HE4 (green); four for the cardiac panel: cTnI (red), CK-MB (green), MYO (blue), and NT-proBNP (yellow). Mean fluorescence intensities (IV) were calculated via the annular ROI method. Error bars show the standard deviation from redundant bead sensors from a single experiment (i.e., the intra-assay standard deviation).

markers like CK-MB and cTnI appear 3 to 6 hours after symptom onset;[53] however, myoglobin has low specificity for cardiac necrosis, necessitating the inclusion of more specific cardiac biomarkers in the final cardiac panel. While the characterization of this full cardiac panel will be presented in future work, here we show initial progress for a rapid myoglobin test on the p-BNC system. In **Fig. 7** the dose response curve for myoglobin shows an excellent fit to the 5-parameter logistic curve (R^2 = 0.9998). Although preliminary in nature, this dose response curve suggests that measurements within the relevant physiological range can be obtained with the low-cost, portable p-BNC system in much less time (7 minutes) than gold-standard reference methods (hours to days).

Conclusions

Here we report the development of a portable, cost-effective, and sensitive detection system that is capable of remote multiplexed and multiclass clinical testing via standardized diagnostic test ensembles that can be quickly customized for new bioscience research and clinical applications. The p-BNC cartridge has successfully transitioned from a prototype device produced in modest volumes to a device designed for mass manufacturing. Further, we designed a portable analyzer intended for non-expert users which fully automates otherwise complex assay protocols, fluid motivation, optical detection, and data analysis. In this report, we have demonstrated the p-BNC's versatility by quantifying eight analytes across three different disease applications. Although preliminary and in need of further characterization in clinical settings, the p-BNC system has the potential to provide quality multiplexed and multiclass POC measurements for a variety of disease applications.

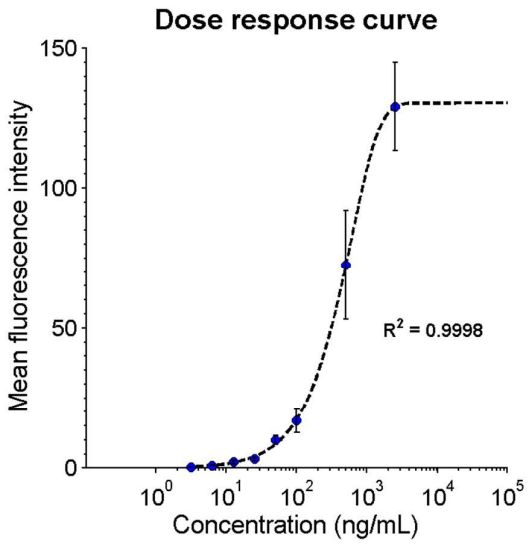

Fig. 7. Rapid myoglobin assay dose response curve shows the MFI for a single run at various dilutions and intra-assay standard deviation from 12-fold bead sensor redundancy (error bars).

Conflicts of interest

Principal Investigator, John T. McDevitt, has an equity interest in SensoDX, LLC. and also serves on the Scientific Advisory Board.

Acknowledgements

Funding was provided by NIH through the National Institute of Dental and Craniofacial Research (NIH Grant No. 3 U01 DE017793-02S1 and 5 U01 DE017793-2). The content is solely the responsibility of the authors and does not necessarily represent or reflect views of the NIH, or the Federal Government. XACTIV (Fairport, NY) is thanked for their assistance in development of the instrumentation enclosure and the mechanical interface.

Notes and references

1. C. D. Chin, V. Linder and S. K. Sia, *Lab Chip*, 2007, **7**, 41-57.
2. P. Yager, T. Edwards, E. Fu, K. Helton, K. Nelson, M. R. Tam and B. H. Weigl, *Nature*, 2006, **442**, 412-418.
3. L. Bissonnette and M. G. Bergeron, *Clin. Microbiol. Infec.*, 2010, **16**, 1044-1053.
4. A. M. Dupuy, S. Lehmann and J. P. Cristol, *Clin. Chem. Lab. Med.*, 2005, **43**, 1291-1302.
5. G. M. Whitesides, *Nature*, 2006, **442**, 368-373.
6. F. B. Myers and L. P. Lee, *Lab Chip*, 2008, **8**, 2015-2031.
7. R. C. R. Wootton and A. J. deMello, *Nature*, 2010, **464**, 839-840.
8. J. West, M. Becker, S. Tombrink and A. Manz, *Anal. Chem.*, 2008, **80**, 4403-4419.
9. C. D. Chin, V. Linder and S. K. Sia, *Lab Chip*, 2012, **12**, 2118-2134.
10. S. O. Kelley, C. A. Mirkin, D. R. Walt, R. F. Ismagilov, M. Toner and E. H. Sargent, *Nat. Nanotechnol.*, 2014, **9**, 969-980.
11. H. A. Stone, A. D. Stroock and A. Ajdari, *Annu. Rev. Fluid Mech.*, 2004, **36**, 381-411.
12. X. Qiu, J. A. Thompson, Z. Chen, C. Liu, D. Chen, S. Ramprasad, M. G. Mauk, S. Ongagna, C. Barber, W. R. Abrams, D. Malamud, P. L. A. M. Corstjens and H. H. Bau, *Biomed. Microdevices*, 2009, **11**, 1175-1186.
13. D. Chen, M. Mauk, X. Qiu, C. Liu, J. Kim, S. Ramprasad, S. Ongagna, W. R. Abrams, D. Malamud, P. L. A. M. Corstjens and H. H. Bau, *Biomed. Microdevices*, 2010, **12**, 705-719.
14. S. Selvakumar, R. Linares, A. Oppenheimer and B. Anthony, *Proc. SPIE, Microfluidics, BioMEMS, and Medical Microsystems X*, 2012, **8251**, 1-6.
15. Abbott Point of Care, Inc., http://www.abbottpointofcare.com/Patient-Care-Settings/Hospital.aspx, (accessed March 25, 2015).
16. Daktari Diagnostics, http://daktaridx.com/products/, (accessed March 25, 2015).
17. J. V. Jokerst, J. W. Jacobson, B. D. Bhagwandin, P. N. Floriano, N. Christodoulides and J. T. McDevitt, *Anal. Chem.*, 2010, **82**, 1571-1579.
18. J. V. Jokerst and J. T. McDevitt, *Nanomedicine*, 2009, **5**, 143-155.
19. C. D. Chin, Y. K. Cheung, T. Laksanasopin, M. M. Modena, S. Y. Chin, A. A. Sridhara, D. Steinmiller, V. Linder, J. Mushingantahe, G. Umviligihozo, E. Karita, L. Mwambarangwe, S. L. Braunstein, J. van de Wijgert, R. Sahabo, J. E. Justman, W. El-Sadr and S. K. Sia, *Clin. Chem.*, 2013, **59**, 629-640.
20. B. S. Lee, Y. U. Lee, H. S. Kim, T. H. Kim, J. Park, J. G. Lee, J. Kim, H. Kim, W. G. Lee and Y. K. Cho, *Lab Chip*, 2011, **11**, 70-78.
21. S. Nie, W. H. Henley, S. E. Miller, H. Zhang, K. M. Mayer, P. J. Dennis, E. A. Oblath, J. P. Alarie, Y. Wu, F. G. Oppenheim, F. F. Little, A. Z. Uluer, P. Wang, J. M. Ramsey and D. R. Walt, *Lab Chip*, 2014, **14**, 1087-1098.
22. K. Choi, A. H. C. Ng, R. Fobel, D. A. Chang-Yen, L. E. Yarnell, E. L. Pearson, C. M. Oleksak, A. T. Fischer, R. P. Luoma, J. M. Robinson, J. Audet and A. R. Wheeler, *Anal. Chem.*, 2013, **85**, 9638-9646.
23. X. Qiu, D. Chen, C. Liu, M. Mauk, T. Kientz and H. Bau, *Biomed. Microdevices*, 2011, **13**, 809-817.
24. A. E. Herr, A. V. Hatch, D. J. Throckmorton, H. M. Tran, J. S. Brennan, W. V. Giannobile and A. K. Singh, *Proc. Natl. Acad. Sci. U. S. A.*, 2007, **104**, 5268-5273.
25. I. K. Dimov, L. Basabe-Desmonts, J. L. Garcia-Cordero, B. M. Ross, A. J. Ricco and L. P. Lee, *Lab Chip*, 2011, **11**, 845-850.
26. F. S. Ligler, K. E. Sapsford, J. P. Golden, L. C. Shriver-Lake, C. R. Taitt, M. A. Dyer, S. Barone and C. J. Myatt, *Anal. Sci.*, 2007, **23**, 5-10.
27. L. Lafleur, D. Stevens, K. McKenzie, S. Ramachandran, P. Spicar-Mihalic, M. Singhal, A. Arjyal, J. Osborn, P. Kauffman, P. Yager and B. Lutz, *Lab Chip*, 2012, **12**, 1119-1127.
28. M. J. Lochhead, K. Todorof, M. Delaney, J. T. Ives, C. Greef, K. Moll, K. Rowley, K. Vogel, C. Myatt, X.-Q. Zhang, C. Logan, C. Benson, S. Reed and R. T. Schooley, *J. Clin. Microbiol.*, 2011, **49**, 3584-3590.
29. M. Xue, W. Wei, Y. Su, J. Kim, Y. S. Shin, W. X. Mai, D. A. Nathanson and J. R. Heath, *J. Am. Chem. Soc.*, 2015, **137**, 4066-4069.
30. Y. Li, J. Xuan, T. Xia, X. Han, Y. Song, Z. Cao, X. Jiang, Y. Guo, P. Wang and L. Qin, *Anal. Chem.*, 2015, **87**, 3771-3777.
31. H. C. Koydemir, Z. Gorocs, D. Tseng, B. Cortazar, S. Feng, R. Y. L. Chan, J. Burbano, E. McLeod and A. Ozcan, *Lab Chip*, 2015, **15**, 1284-1293.
32. N. L. Dell, S. Venkatachalam, D. Stevens, P. Yager and G. Borriello, *Proceedings of the 5th ACM workshop on networked systems for developing regions*, 2011, 3-8.
33. A. Nemiroski, D. C. Christodouleas, J. W. Hennek, A. A. Kumar, E. J. Maxwell, M. T. Fernández-Abedul and G. M. Whitesides, *Proc. Natl. Acad. Sci. U. S. A.*, 2014, **111**, 11984-11989.
34. S. Wang, X. Zhao, I. Khimji, R. Akbas, W. Qiu, D. Edwards, D. W. Cramer, B. Ye and U. Demirci, *Lab Chip*, 2011, **11**, 3411-3418.
35. P. S. Dittrich, K. Tachikawa and A. Manz, *Anal. Chem.*, 2006, **78**, 3887-3908.
36. A. M. Amin, R. Thakur, S. Madren, H. S. Chuang, M. Thottethodi, T. N. Vijaykumar, S. T. Wereley and S. C. Jacobson, *Microfluid. Nanofluid.*, 2013, **15**, 647-659.
37. J. V. Jokerst, J. Chou, J. P. Camp, J. Wong, A. Lennart, A. A. Pollard, P. N. Floriano, N. Christodoulides, G. W. Simmons,

Y. Zhou, M. F. Ali and J. T. McDevitt, *Small*, 2011, **7**, 613-624.
38. J. V. Jokerst, A. Raamanathan, N. Christodoulides, P. N. Floriano, A. A. Pollard, G. W. Simmons, J. Wong, C. Gage, W. B. Furmaga, S. W. Redding and J. T. McDevitt, *Biosens. Bioelectron.*, 2009, **24**, 3622-3629.
39. P. N. Floriano, N. Christodoulides, C. S. Miller, J. L. Ebersole, J. Spertus, B. G. Rose, D. F. Kinane, M. J. Novak, S. Steinhubl, S. Acosta, S. Mohanty, P. Dharshan, C. K. Yeh, S. Redding, W. Furmaga and J. T. McDevitt, *Clin. Chem.*, 2009, **55**, 1530-1538.
40. W. R. Rodriguez, N. Christodoulides, P. N. Floriano, S. Graham, S. Mohanty, M. Dixon, M. Hsiang, T. Peter, S. Zavahir, I. Thior, D. Romanovicz, B. Bernard, A. P. Goodey, B. D. Walker and J. T. McDevitt, *PLoS Med.*, 2005, **2**, 0663-0672.
41. B. H. Shadfan, A. R. Simmons, G. W. Simmons, A. Ho, J. Wong, K. H. Lu, R. C. Bast, Jr. and J. T. McDevitt, *Cancer Prev. Res.*, 2015, **8**, 37-48.
42. J. Chou, J. Wong, N. Christodoulides, P. Floriano, X. Sanchez and J. McDevitt, *Sensors*, 2012, **12**, 15467-15499.
43. J. Chou, N. Du, T. Ou, P. N. Floriano, N. Christodoulides and J. T. McDevitt, *Biosens. Bioelectron.*, 2013, **42**, 653-660.
44. J. Chou, A. Lennart, J. Wong, M. F. Ali, P. N. Floriano, N. Christodoulides, J. Camp and J. T. McDevitt, *Anal. Chem.*, 2012, **84**, 2569-2575.
45. J. Chou, L. E. Li, E. Kulla, N. Christodoulides, P. N. Floriano and J. T. McDevitt, *Lab Chip*, 2012, **12**, 5249-5256.
46. A. Rhodes and L. Bai, *Proceedings of the British Machine Vision Conference*, 2011, 1-11.
47. L. Shen and L. Bai, *Pattern Anal. Appl.*, 2006, **9**, 273-292.
48. N. Christodoulides, R. De La Garza, II, G. W. Simmons, M. P. McRae, J. Wong, T. F. Newton, R. Smith, J. J. Mahoney Iii, J. Hohenstein, S. Gomez, P. N. Floriano, H. Talavera, D. J. Sloan, D. E. Moody, D. M. Andrenyak, T. R. Kosten, A. Haque and J. T. McDevitt, *Drug Alc. Dep.*, 2015, **153**, 306-313.
49. N. Christodoulides, F. N. Pierre, X. Sanchez, L. Li, K. Hocquard, A. Patton, R. Muldoon, C. S. Miller, J. L. Ebersole, S. Redding, C.-K. Yeh, W. B. Furmaga, D. A. Wampler, B. Bozkurt, C. M. Ballantyne and J. T. McDevitt, *Methodist DeBakey Cardiovasc. J.*, 2012, **8**, 6-12.
50. M. J. Stone, M. R. Waterman, D. Harimoto, G. Murray, N. Willson, M. R. Platt, G. Blomqvist and J. T. Willerson, *Brit. Heart J.*, 1977, **39**, 375-380.
51. M. Plebani and M. Zaninotto, *Clin. Chim. Acta*, 1998, **272**, 69-77.
52. L. E. Roxin, I. Cullhed, T. Groth, T. Hällgren and P. Venge, *Acta Med. Scand.*, 1984, **215**, 417-425.
53. J. McCord, R. M. Nowak, P. A. McCullough, C. Foreback, S. Borzak, G. Tokarski, M. C. Tomlanovich, G. Jacobsen and W. D. Weaver, *Circulation*, 2001, **104**, 1483-1488.